



Full Length Article

Development of novel biofilm using *Musa acuminata* (waste banana leaves) mediated biogenic zinc oxide nanoparticles reinforced with chitosan blend

Shivtraloshini Sasidharan^a, Lai-Hock Tey^a, Sinouvassane Djearamane^b,
Nor Khaizura Mahmud Ab Rashid^c, Raajeswari PA^d, Ling Shing Wong^{e,*},
Anto Cordelia Tanislaus Antony Dhanapal^{a,*}

^a Department of Chemical Science, Faculty of Science, Universiti Tunku Abdul Rahman, Kampar 31900 Malaysia

^b Department of Allied Health Sciences, Faculty of Science, Universiti Tunku Abdul Rahman (UTAR), Kampar 31900, Malaysia; Biomedical Research Unit and Lab Animal Research Centre, Saveetha Dental College, Saveetha Institute of Medical and Technical Sciences, Saveetha University, Chennai 602105, India

^c Department of Food Science, Faculty of Food Science and Technology, University Putra Malaysia, 43400 UPM Serdang, Selangor, Malaysia

^d Department of Food Science and Nutrition, Avinashilingam Institute for Home Science and Higher Education for Women, Coimbatore, Tamil Nadu, India

^e Life Science Division, Faculty of Health and Life Sciences, INTI International University, Nilai 71800, Malaysia

ARTICLE INFO

Keywords:

Antibacterial
Musa acuminata
Biogenic ZnO NP
Chemogenic ZnO NP
Food packaging biofilm
Green product

ABSTRACT

Objectives: The present study reports a cost-effective, eco-friendly, and straightforward approach to synthesize Zinc Oxide Nanoparticles (ZnO NPs) using agro-waste banana (*Musa acuminata*) leaves and compares it with chemogenic ZnO NP.

Methods: The study investigated biogenic and chemogenic ZnO NPs, examining their size, shape, morphological structure, and stability using UV-Vis Spectroscopy, X-Ray Diffraction (XRD), Field Transmission Scanning Electron Microscopy (FESEM), Energy Dispersive X-Ray (EDX), and Fourier Transform Infrared Spectroscopy (FTIR). Antibacterial potency against *Staphylococcus aureus* and *Salmonella typhimurium* was tested through the Disk Diffusion method. Bio-nanocomposites were created by incorporating different ZnO NP concentrations into chitosan via the solvent casting method. Film characteristics were analyzed using SEM, tensile strength, film moisture (FM), film solubility (FS), and water-holding capacity (WHC). Antibacterial activity of the bio-nanocomposites was assessed against *Staphylococcus aureus* and *Salmonella typhimurium* using the Viable Cell Colony Count method.

Results: The results of color change confirmed the formation of biogenic and chemogenic ZnO NP having sharp peaks at 370 nm and 381 nm respectively having spherical structure with an average crystalline size of 36.73 nm and 75.31 nm. The biogenic ZnO NP had greater inhibitory action against both *Staphylococcus aureus* and *Salmonella typhimurium* than chemogenic ZnO NP. Besides, the biogenic biofilms had enhanced characteristics followed by chemogenic and chitosan biofilms.

Conclusion: The study suggests a green approach, using smaller nanosized biogenic ZnO NPs with unique advantages over chemogenic counterparts. The resulting biofilms exhibit the potential to enhance food quality, safety, and longevity in the food industry. This aligns with circular green economy principles, utilizing waste banana leaves for raw material synthesis and promoting manufacturing innovation.

1. Introduction

Musa acuminata is a species of banana native to Southern Asia specific to Musaceae from the Plantae family. It is the second-highest production after citrus and the fourth-highest food crop after rice, wheat, and corn (Alzate Acevedo et al., 2021). In Malaysia alone, bananas cover

26,000 ha, yielding 530,000 metric tonnes annually (Tan, 2022). Banana fruits once in a lifespan of 10 to 12 months from planting to harvest. After harvesting, the tree is cut, leaving the stem and rhizome for new growth (Abdul Razak et al., 2021). Producing 100 kg of rejected fruit and about 4 tonnes of waste generation per tonne (Mohd Taib et al., 2014). The massive waste becomes a valuable resource for various

* Corresponding authors at: INTI International University, Persiaran Perdana BBN, 71800 Nilai, Negeri Sembilan, Malaysia (L.S. Wong). Block D, 124F, Faculty of Science, Universiti Tunku Abdul Rahman, Kampar, 31900 Malaysia (A.C.T.A. Dhanapal).

E-mail addresses: lingshing.wong@newinti.edu.my (L. Shing Wong), antoc@utar.edu.my (A.C. Tanislaus Antony Dhanapal).

<https://doi.org/10.1016/j.jksus.2023.103080>

Received 14 September 2023; Received in revised form 5 December 2023; Accepted 24 December 2023

Available online 27 December 2023

1018-3647/© 2023 The Authors. Published by Elsevier B.V. on behalf of King Saud University. This is an open access article under the CC BY-NC-ND license (<http://creativecommons.org/licenses/by-nc-nd/4.0/>).

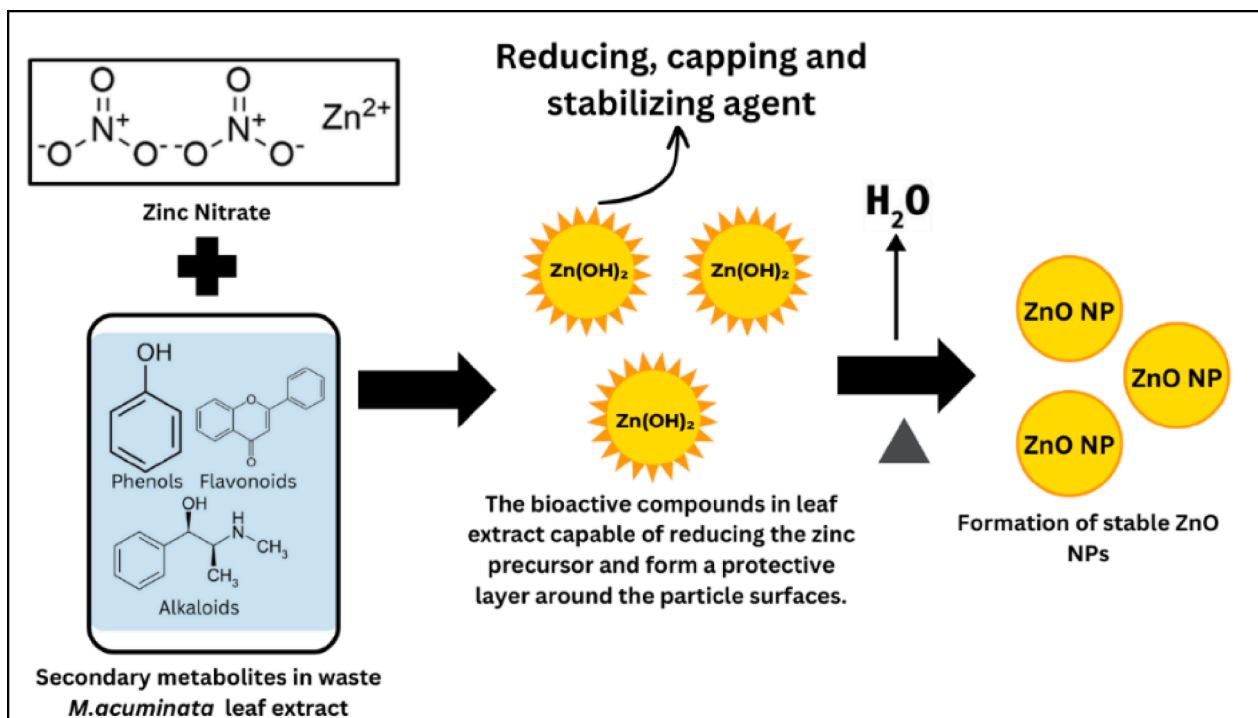


Fig. 1. Bioactive compounds in the waste *M. acuminata* leaf extract that act as reducing, capping, and stabilizing agents.

industries. Banana processing agro-waste contributes to renewable energy, nanotechnology, and the production of biodegradable plastics for a sustainable circular economy (Alzate Acevedo et al., 2021). The circular economy maximizes natural resource use, sustains value, reduces waste, and operates self-contained production cycles, aligning with social and environmental regulations, presenting a novel, eco-friendly, and economically efficient solution, easing global economic pressures. (Alzate Acevedo et al., 2021).

Nanotechnology involves manipulating materials at the nanoscale (below 100 nm), merging scientific disciplines for broad technology applications. (Kaushik et al., 2010). Nanoparticle synthesis involves “Bottom-Up” creation via oxidation or reduction for nanoscopic entities and “Top-Down” methods using mechanical processes to break down larger materials into nanoparticles. These strategies, relying on extensive chemicals, lead to imperfect surface structures and pose environmental hazards (Azim et al., 2022). The biological approach surpasses traditional methods in nanoparticle synthesis, offering eco-friendly, efficient, and cost-effective benefits while imparting remarkable properties to nanoparticles (Imade et al., 2022). Plants contribute biomolecules for nanoparticle synthesis, playing a crucial role in reducing, capping, and stabilizing nanoparticles (Basnet et al., 2018). ZnO NPs, a promising metal oxide, exhibit unique properties as effective antimicrobial agents, active catalysts, and hold potential applications in medicinal fields (Kalpana & Devi Rajeswari, 2018). Bio-nanocomposites, gaining recent attention, blend natural polymers and nanoparticles for outstanding properties. Chitosan is the second most abundant bio-based polymer derived from the deacetylation of chitin in crustaceans, arthropods, and fungi cell walls. (Rahman et al., 2017). Chitosan was chosen for its non-toxicity, biocompatibility, biodegradability, and antimicrobial properties, and approved as a food additive by the Food and Drug Administration (FDA) in developing biodegradable food packaging (Terzioğlu et al., 2021). Fig. 1 illustrates the mechanism of action of the bioactive compounds that act as reducing, capping and stabilizing agent.

Herein, this present study focuses on a facile, green, and economically efficient method for preparing stable ZnO NP by waste banana (*Musa acuminata*) leaf extract without any addition of chemicals. This

study is the first in the available literature, proposing that waste *Musa acuminata* leaves after fruiting act as reducing and surface stabilizing agents in synthesizing highly pure ZnO NPs. Both biogenic and chemogenic ZnO NPs were characterized using UV-Vis, XRD, SEM, EDX, and FTIR. Antibacterial properties were assessed against *Salmonella typhimurium* and *Staphylococcus aureus* via the Disk Diffusion method. Nanotechnology was applied to create bio-nanocomposites by incorporating ZnO NPs into a chitosan matrix, enhancing biofilm properties. The biofilm’s morphology, tensile grip, FM, FS, and WHC were evaluated. Results suggest potential commercialization in the food industry for chitosan incorporated with ZnO NPs.

2. Material and methods

Zinc Nitrate ($\text{Zn}(\text{NO}_3)_2$), Potassium Hydroxide (KOH), ethanol, and glycerol were obtained from Synertec Enterprise (Malaysia), Iron Chloride (FeCl_3) and Lead Acetate ($\text{Pb}(\text{C}_2\text{H}_3\text{O}_2)_2$) were acquired from Medigene (Malaysia), Sodium Hydroxide (NaOH), Hydrochloric Acid (HCl), Sodium Chloride (NaCl), and glacial acetic acid were purchased from Labmedical Science (Malaysia) and lastly chitosan (high molecular weight of 31–37 kDa) with deacetylation process of 75% was obtained from PremierDiagnostics (Malaysia), deionized water. All the microbial reagents were purchased from Fc. Bios. Sdn. Bhd. (Malaysia): *Staphylococcus aureus* (ATCC® 6538TM), Mueller-Hinton Agar (MHA), Tryptic Soy Broth (TBA), and Tryptic Soy Agar (TSA). All chemicals used were either of analytical or reagent grade. The methodology overview is shown in Fig. 2.

2.1. Preparation of waste banana (*Musa acuminata*) leaves using aqueous extraction

The waste *M. acuminata* leaves from Agriculture Park, UTAR were washed, cut, and dried in an oven for 3 days at 60 °C. The dried leaves were ground into a fine powder and stored at 4 °C. Aqueous extraction involved mixing 40 g of the powder with 400 mL of deionized water, leaving it overnight, and then filtering using a vacuum filter. The resulting extract was refrigerated at 4 °C for further use (Jayachandran

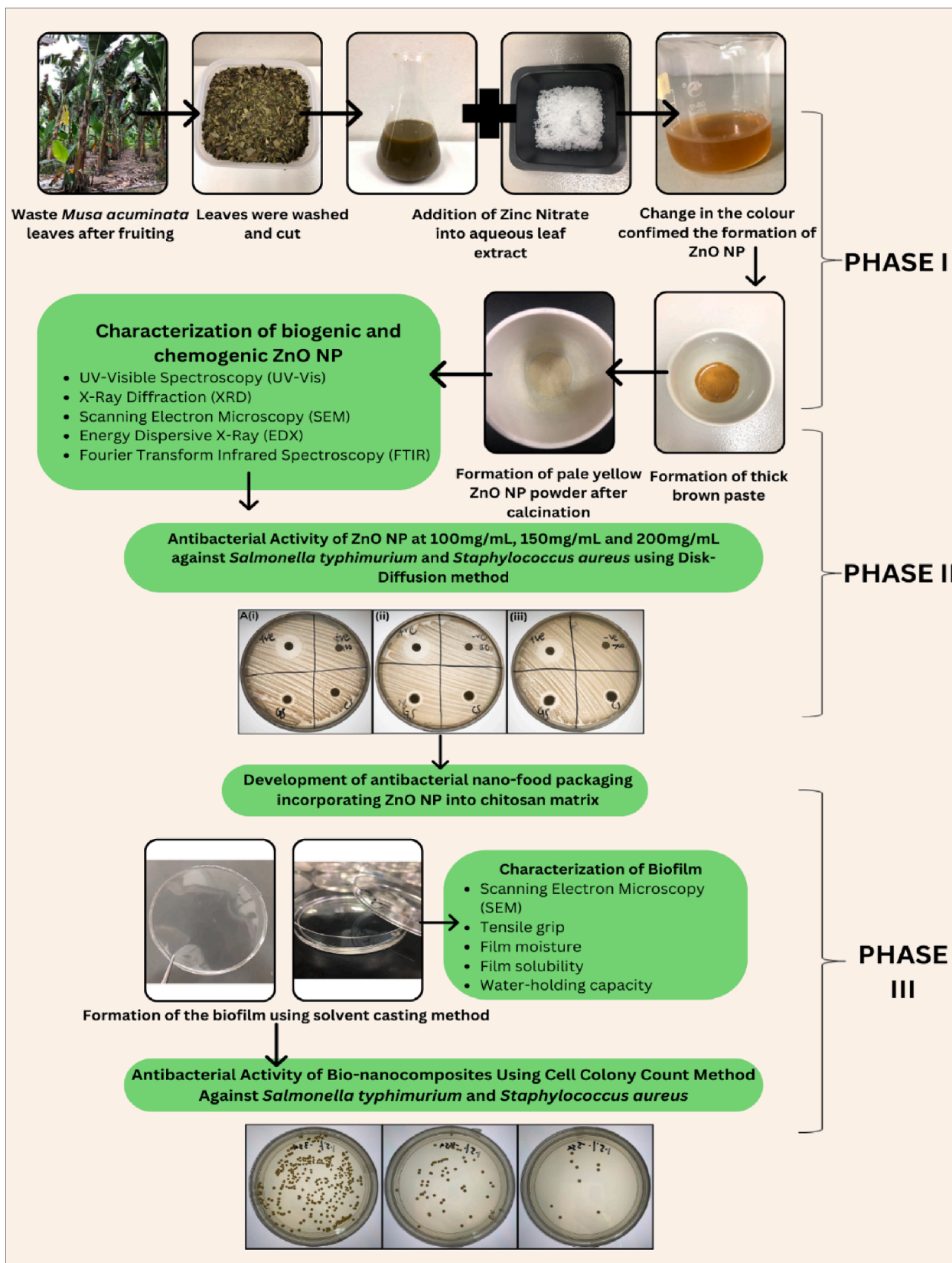


Fig. 2. The overview of the study.

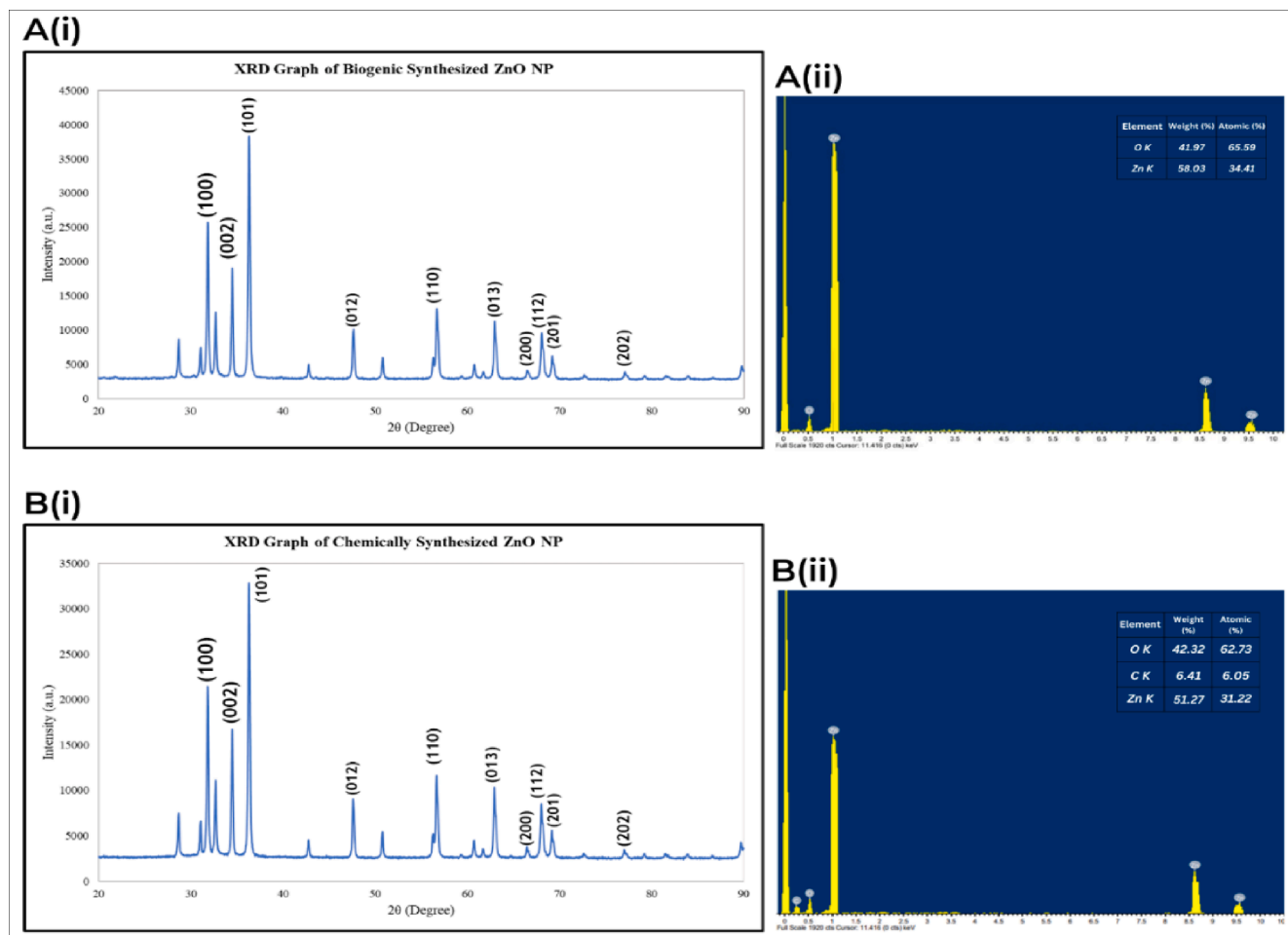


Fig. 3. (A(i), B(i)) XRD graph of biogenic and chemogenic ZnO NP, (A(ii), B(ii)) Compositional analysis of biogenic and chemogenic ZnO NP.

et al., 2021).

2.2. Phytochemical screening

The aqueous leaf extract of waste *M. acuminata* was screened for the presence of phytonutrients like phenols, flavonoids, alkaloids, tannins, terpenoids, saponins, glycosides, and reducing sugar.

2.3. Synthesis of ZnO NPs (Emamifar et al., 2010)

2.3.1. Green synthesis of ZnO NP

2 g Zinc Nitrate was added to 30 mL waste *M. acuminata* leaf extract and heated at 60 °C until a dark brown paste formed. This paste was calcinated at 400 °C for 2 h, resulting in faded white ZnO NP powder.

2.3.2. Chemical synthesis of ZnO NP

The 0.2 M Zinc Nitrate was mixed with 0.4 M Potassium Hydroxide for an hour, followed by centrifugation at 5000 rpm for 20 min. After washing, the white paste was calcinated at 400 °C for 2 h, producing white ZnO NP powder.

2.4. Characterization of ZnO NPs (Tan et al., 2023)

2.4.1. UV-Vis Spectroscopy

UV-vis absorption spectra were recorded at room temperature using a GENESYS 180 UV-vis spectrophotometer, measuring transmittance at wavelengths from 300 nm to 800 nm for biogenic and chemogenic ZnO NPs suspensions.

2.4.2. Field Transmission Scanning Electron Microscopy (FESEM)

Structural analysis and composition were performed using FESEM with EDX. ZnO NPs were observed using a JEOL JSM-6400 SEM at 15 kV. Before analysis, samples were coated with gold using a Bio-rad system for 3 min for proper conductivity.

2.4.3. X-Ray diffraction (XRD)

The crystallinity index of ZnO NPs was determined from XRD patterns using a Philips/X'Pert Pro Panalytical-PW 3040/60 MPD diffractometer. Scans were conducted at a rate of 2 per minute within an angle range of 20° to 90°. The crystallinity index (CIr) was calculated using a specific formula:

$$CIr(\%) = \frac{(I_{002} - I_{am})}{I_{002}} \times 100$$

CIr: Corrosion Inhibition Efficiency in percentage.

I002: Initial corrosion rate without inhibition (absent of corrosion inhibitor).

Iam: Corrosion rate with inhibition (present of corrosion inhibitor).

2.4.4. Fourier transform infrared (FTIR) Spectroscopy

FTIR analysis of ZnO NPs was conducted using a Fourier transform infrared spectrophotometer from Kyoto, Japan. KBr served as a carrier for IR spectrum samples, and the analysis spanned the range of 400 cm⁻¹ to 4000 cm⁻¹.

2.5. Antimicrobial study of ZnO NP and packaging films

The antimicrobial activity of ZnO NPs against *Staphylococcus aureus*,

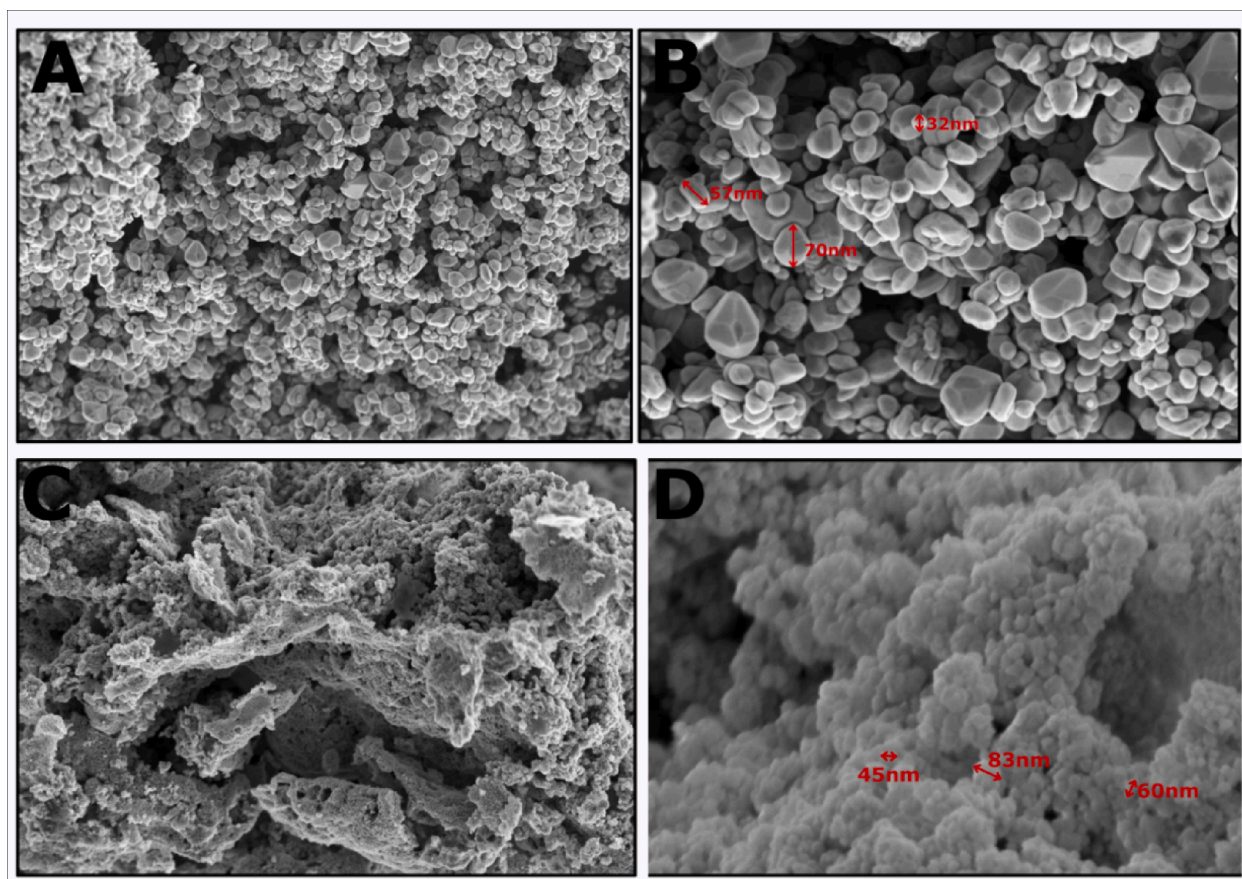


Fig. 4. Morphological structure of (A, B) biogenic ZnO NP, (C, D) chemogenic ZnO NP.

Gram-positive bacterium (ATCC® 6538™), and *Salmonella typhimurium*, Gram-negative bacterium (ATCC® 14028™) was assessed using the Disk Diffusion method. MHA agar plates were inoculated with bacteria, and filter papers soaked in 100 mg/mL, 150 mg/mL, and 200 mg/mL ZnO NPs were placed on the agar. Controls included penicillin (positive) and deionized water (negative). After incubation at 37 °C for 20 h, inhibition zone diameters were measured and presented in cm.

The antimicrobial potency of bio-nanocomposites was assessed via the Viable Cell Colony Count (CFU) method against the strains above. Each 0.1 g film was placed in Tryptic Soy Broth with bacteria and incubated at 37 °C for 24 h. Controls included tubes without films (blank) and pristine chitosan film. After plating on Tryptic Soy Agar of each serial dilution and incubation, colonies were counted, and log reductions were calculated.

Number of log reductions = $\log B - \log A$

Whereby, B and A are the mean number of bacteria (CFU/mL) in tubes labeled as blank and conditioned samples after 24-hour incubation.

2.6. Preparation of Bio-nanocomposites

Chitosan films were prepared by dissolving chitosan 1.5% (w/v) in 1% glacial acetic acid (v/v) with constant stirring. Biogenic and chemogenic ZnO NPs (0.5%, 1%, 1.5%, 2%, and 2.5%) were added and the mixture was cast in a petri dish and dried for 24 h, with pristine chitosan as the control (Souza et al., 2020b).

2.7. Characterization of biofilms (Liu et al., 2021)

All the characterization was repeated on chemogenic films.

2.7.1. Field Transmission Scanning Electron Microscopy (FESEM)

Film surface and cross-section were captured using the Zeiss DSM 962 instrument (Germany) in a vacuum (3 kV acceleration).

2.7.2. Tensile grip

Tensile strength was measured with a TA. XT-plus texture analyzer (Stable Micro Systems Ltd., UK) for films cut into 6 cm × 3 cm, with a crosshead movement at 32 mm/min.

2.7.3. Film solubility

Films (3cmx3cm) were immersed in 200 mL deionized water and heated at 80 °C for 3 h, followed by drying at 100 °C for 24 h. Initial and final weights were recorded, and the FS (%) was calculated accordingly.

$$FS (\%) = ((W_i - W_f)/W_i) \times 100\%$$

2.7.4. Film moisture

The initial weight of the biofilm was recorded (3cmx3cm). The biofilms were kept in an oven at 110 °C for 24 h and the final weight was recorded. The FM (%) was calculated using the formula stated below:

$$MC (\%) = ((W_f - W_i)/W_f) \times 100\%$$

2.7.5. Water-holding capacity

Biofilms (3 cm × 3 cm) were initially weighed, immersed in 200 mL deionized water for 30 min, and pressed with filter paper to remove excess water. The final weight was recorded, and the WHC (%) was calculated using the provided formula.

$$WHC (\%) = ((W_f - W_i)/W_f) \times 100\%$$

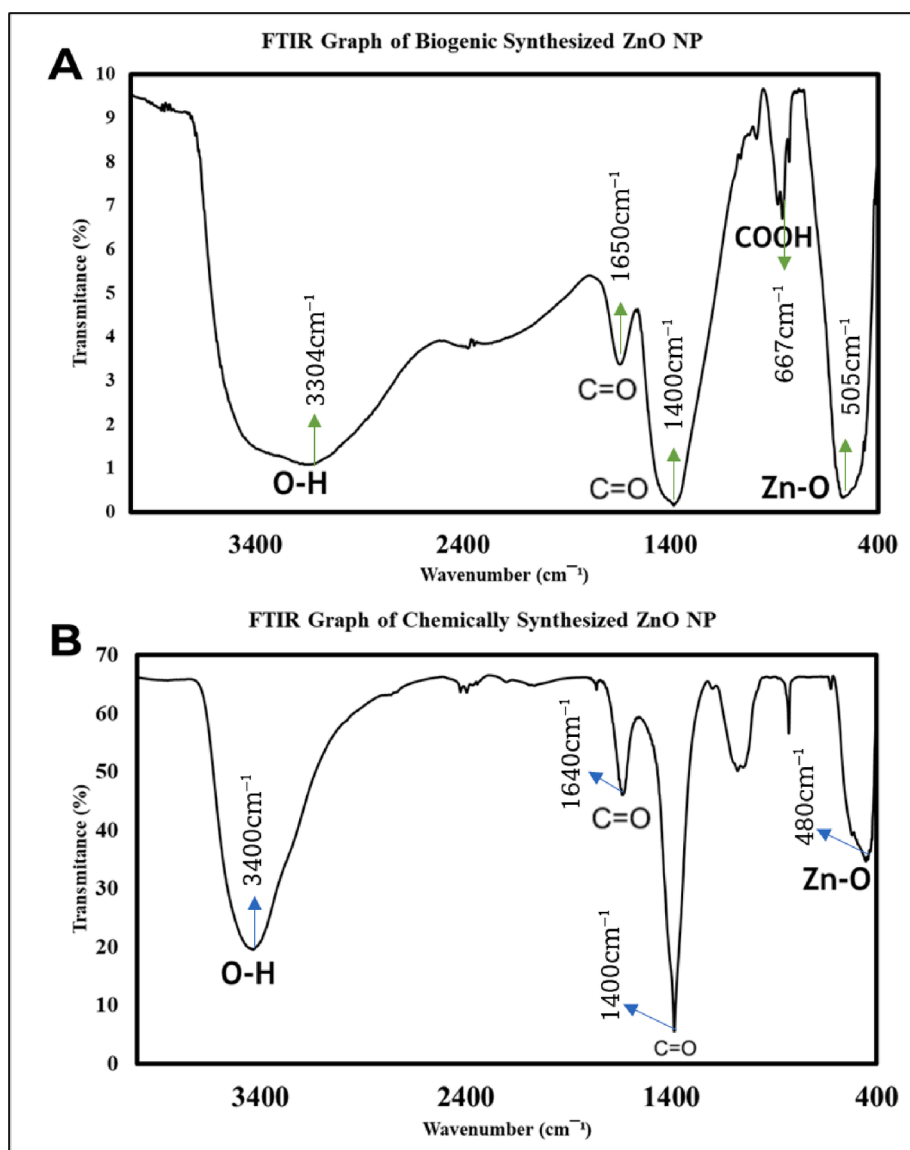


Fig. 5. Functional groups of (A) biogenic ZnO NP, (B) chemogenic ZnO NP.

2.8. Statistical analysis

Statistical analysis involved one-way analysis of variance using SPSS 22 Software. Mean value variations were assessed with the Tukey test, and significance was set at $p < 0.05$.

3. Results and discussion

3.1. Characterization of biogenic and chemogenic ZnO NP

3.1.1. UV-Vis Spectroscopy

Plant secondary metabolites aid in reducing Zn²⁺ ions to ZnO, forming a protective layer around nanoparticles. The plant extract serves as both reducing and stabilizing agents, confirmed through UV-visible spectrum analysis (300 nm to 800 nm) (Velumani et al., 2022). The biogenic and chemogenic ZnO NP spectrum exhibited peaks at 370 nm and 381 nm respectively, aligning with ZnO NP specifications (Basnet et al., 2018). The optical band gap energy at the highest absorption peak for biogenic and chemogenic ZnO NPs was 3.32 eV and 3.13 eV respectively. A higher band gap energy suggests a smaller crystallite size, with lower wavelength values indicating higher energy

absorption and a higher bandgap (Youssef A. et al., 2015).

3.1.2. X-Ray diffraction (XRD), Scanning Electron Microscopy (SEM), and energy Dispersive X-Ray (EDX)

The crystallinity and the average crystallite size of ZnO NP were evaluated using the X-Ray diffraction technique (XRD). The XRD pattern of biogenic and chemogenic ZnO NP reveals sharp peaks of the crystalline nature and the phase purity of the sample. The diffraction peaks of biogenic ZnO NP at 2θ values 31.80°, 34.46°, 36.29°, 42.74°, 50.76°, 61.68°, 62.92°, 66.45°, 69.15° corresponding to the (100), (002), (101), (012), (110), (013), (200), (112), (201) and (202) crystal planes respectively whereas the diffraction peaks of chemogenic ZnO NP at 2θ values are 31.80°, 34.46°, 36.29°, 42.75°, 50.76°, 60.70°, 61.69°, 62.92°, 66.44°, and 69.15° aligned with crystal planes at (100), (002), (101), (012), (110), (013), (200), (112), (201) and (202) respectively. The planes of biogenic and chemogenic ZnO NP are matched with the standard database (ICDD 01-079-5604) and (ICDD 01-070-2551) respectively and presented in a spherical structure. Scherrer's formula was used to calculate the mean crystalline size of biogenic and chemogenic ZnO NP as below:

$$D = K\lambda / (\beta \cos\theta)$$

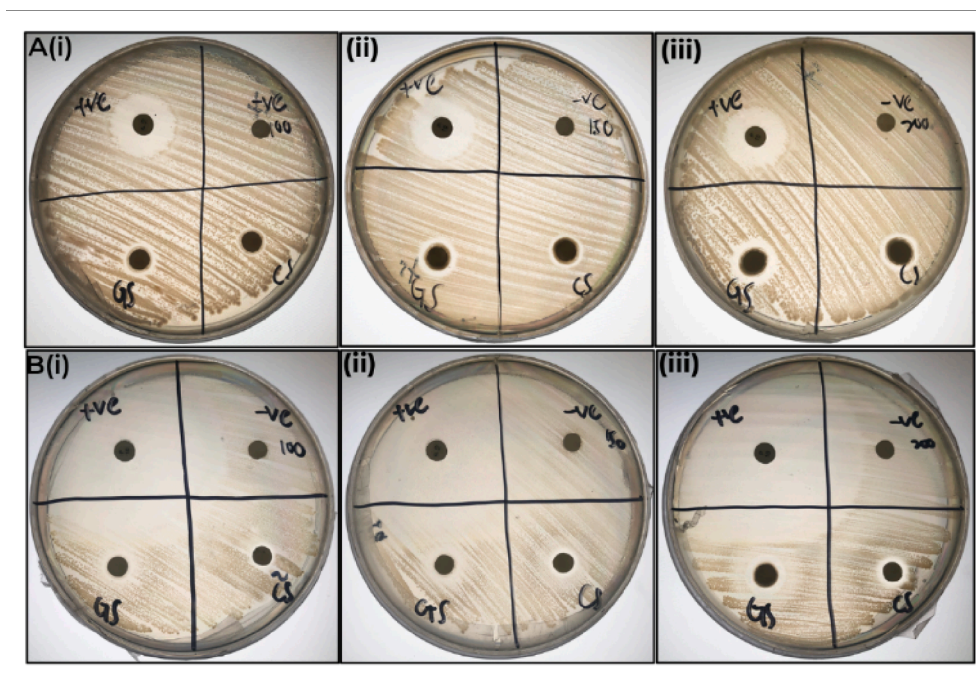


Fig. 6. Study of inhibitory action of ZnO NP against *S. aureus* and *S. typhimurium*: the subset of (A(i), (ii), (iii)) the zone of inhibition of biogenic and chemogenic ZnO NP against *S. typhimurium* at 100 mg/mL, 150 mg/mL and 200 mg/mL, the subset of (B(i), (ii), (iii)) the zone of inhibition of biogenic and chemogenic ZnO NP against *S. aureus* at 100 mg/mL, 150 mg/mL and 200 mg/mL.

Table 1

The zone of inhibition of biogenic and chemogenic ZnO NP against *S. aureus* and *S. typhimurium*.

Samples	Inhibition zone (cm)		
	100 mg/mL	150 mg/mL	200 mg/mL
<i>Staphylococcus aureus</i>			
Penicillin	4.931 ± 0.0312	4.377 ± 0.0114	4.573 ± 0.0223
Deionized water	0.000	0.000	0.000
Biogenic ZnO NP	1.000 ± 0.0122	1.177 ± 0.033	1.235 ± 0.0200
Chemogenic ZnO NP	0.685 ± 0.0193	0.823 ± 0.023	1.038 ± 0.0153
<i>Salmonella typhimurium</i>			
Penicillin	1.702 ± 0.0112	1.872 ± 0.0224	1.80 ± 0.011
Deionized water	0.000	0.000	0.000
Biogenic ZnO NP	0.801 ± 0.0214	1.131 ± 0.0383	1.172 ± 0.0188
Chemogenic ZnO NP	0.572 ± 0.0195	0.701 ± 0.0330	0.935 ± 0.0291

Where D is the average crystalline size (nm), K is the shape factor (0.9), λ is the incident radiation wavelength (1.54 Å), β is the full width at half maximum (FWHM), and θ is the diffraction angle. The average crystalline size of the biogenic and chemogenic ZnO NP was 36.73 nm and 75.31 nm.

Surface morphology and compositional analysis of biogenic and chemogenic ZnO NPs were performed using SEM and EDX. Fig. 4 displays spherical nanoparticles with smooth surfaces and even distribution. EDX confirms the presence of Zinc in oxide form, with strong peaks for Zinc (1 eV, 8.6 eV, 9.5 eV) and Oxygen (0.5 eV). Biogenic ZnO NPs exhibit a pure composition, showing only Zinc and Oxygen peaks, indicating their purity (Figs. 3 and 4) (Jayachandran et al., 2021b).

3.1.3. Fourier transform infrared Spectroscopy (FTIR)

FTIR identifies functional groups in ZnO NPs responsible for synthesis and stabilization, with peaks associated with bioactive compounds from the plant extract. The absorption band from 1400 cm to 1 to 3444 cm⁻¹ in the FTIR spectrum corresponds to H-O-H bending vibrations of water molecules (Mahdi Ismail et al., 2023). Aromatic C-H vibrations are observed in the range of 2900 cm⁻¹ to 3100 cm⁻¹, while the

absorption band at 510 cm⁻¹ to 400 cm⁻¹ reflects Zn-O stretching vibrations (Mahdi Ismail et al., 2023).

In the FTIR spectrum (Fig. 5) of biogenic ZnO NPs, the broadband at 3304 cm⁻¹ indicates O-H stretching of phenolic compounds. Bands at 1650 cm⁻¹ and 1400 cm⁻¹ correspond to C = O bond stretching, while 667 cm⁻¹ signifies the COOH bond, and 505 cm⁻¹ suggests Zn-O stretching. In chemogenic ZnO NPs, the band at 3400 cm⁻¹ represents the O-H group, 1640 cm⁻¹ and 1400 cm⁻¹ show the CO-OH group, and 480 cm⁻¹ indicates Zn-O stretching. The hydroxyl group (-OH) from phenolic and flavonoid contents in both NPs acts as a reducing agent, aiding Zn²⁺ ion reduction to Zn⁰ atoms, preventing agglomeration (Jayachandran et al., 2021; Yashni, G. et al., 2019).

3.2. Antimicrobial properties of ZnO NP and packaging Films.

The disk-diffusion test was carried out against *S. typhimurium* and *S. aureus* whereby the result obtained was the formation of a concentration-dependent inhibition zone (Fig. 6, Table 1). The maximum inhibitory action of both biogenic and chemogenic ZnO NPs against *S. typhimurium* and *S. aureus* was seen in the highest concentration (200 mg/mL) whereas minimum inhibitory action of biogenic and chemogenic ZnO NP against *S. typhimurium* and *S. aureus* was observed in the lowest concentration (100 mg/mL). A larger inhibition zone was observed in Gram-positive bacteria *S. aureus* compared to Gram-negative bacteria *S. typhimurium*. The thicker outer cell membrane in *S. typhimurium* contributes to its resistance to both biogenic and chemogenic ZnO NPs (Tian F. et al., 2019).

The bio-nanocomposite's antimicrobial activity against both bacteria strains revealed the highest microbial growth in the chitosan film ($p < 0.05$). The log reduction was more pronounced in contact with *S. typhimurium* (Gram-negative) compared to *S. aureus* (Gram-positive) (Fig. 7). Chitosan's antimicrobial mechanism involves interaction between its positively charged amino groups and microbial membranes, disrupting permeability, and causing material leakage, leading to microbial death. Chitosan's ability to chelate metals further inhibits essential nutrient flow, impacting metabolism. Gram-positive bacteria are more susceptible due to their lack of an outer membrane, while

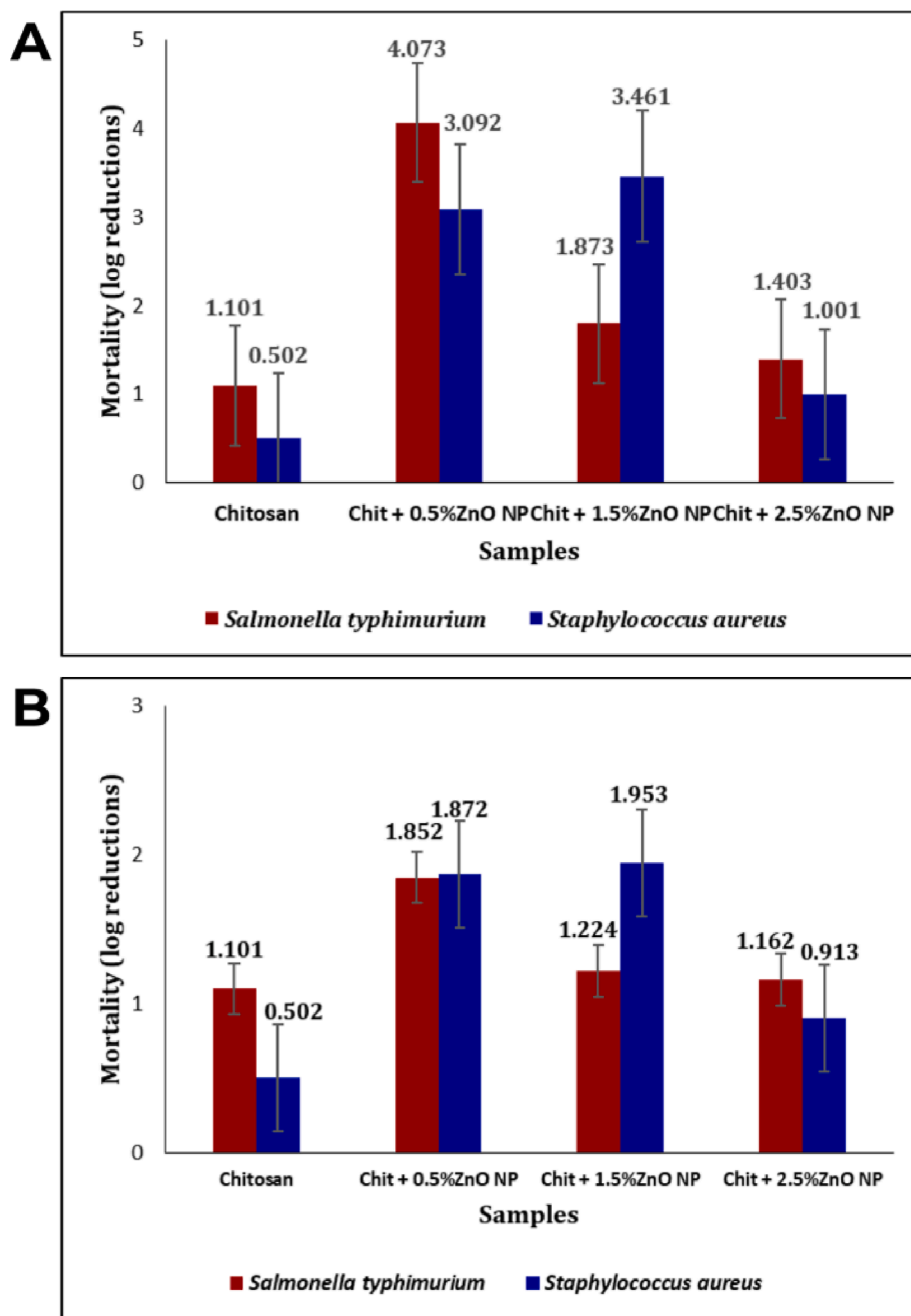


Fig. 7. Antibacterial activity of bio-nanocomposites.

Gram-negative bacteria, possessing this extra layer, exhibit greater resistance.

The incorporation of ZnO NPs significantly altered chitosan's antimicrobial properties against respective bacteria ($p < 0.05$). For biogenic ZnO NPs, *S. typhimurium* showed decreased mortality rates, with the most significant effect at 0.5% concentration. In *S. aureus*, mortality rates were enhanced at lower ZnO NP levels (0.5% and 1.5%), but log reduction decreased at 2.5% compared to 1.5%. For chemogenic ZnO NPs, *S. typhimurium* displayed a decreasing mortality rate, while *S. aureus* showed an increasing mortality rate at the first two concentrations (0.5% and 1.5%), with lower log reduction at 2.5% compared to 1.5%. Similar to biogenic NPs, log reductions for 1.5% ZnO NPs were higher for *S. aureus* than for *S. typhimurium*.

The antibacterial effectiveness of chitosan films decreases with the addition of ZnO NPs, impacting their overall antimicrobial significance.

Reduced ZnO NP size improves antimicrobial efficacy by releasing Zn^{2+} upon light exposure, leading to Reactive Oxygen Species (ROS) formation on bacterial cell walls, ultimately causing cell destruction. While Gram-negative bacteria like *S. typhimurium* are susceptible, Gram-positive *S. aureus* exhibits higher resistance due to antioxidant content. ZnO NPs' affinity for *S. typhimurium* induces cell membrane damage, affecting ROS susceptibility and antimicrobial activity. However, increased ZnO NP concentration may lead to agglomeration, diminishing bio-nanocomposite antimicrobial efficacy.

3.3. Characterization of chitosan - biogenic and chemogenic ZnO NP food packaging film

3.3.1. Scanning Electron Microscopy (SEM)

Chitosan film remained smooth, crack-free, and bubble-free. Adding

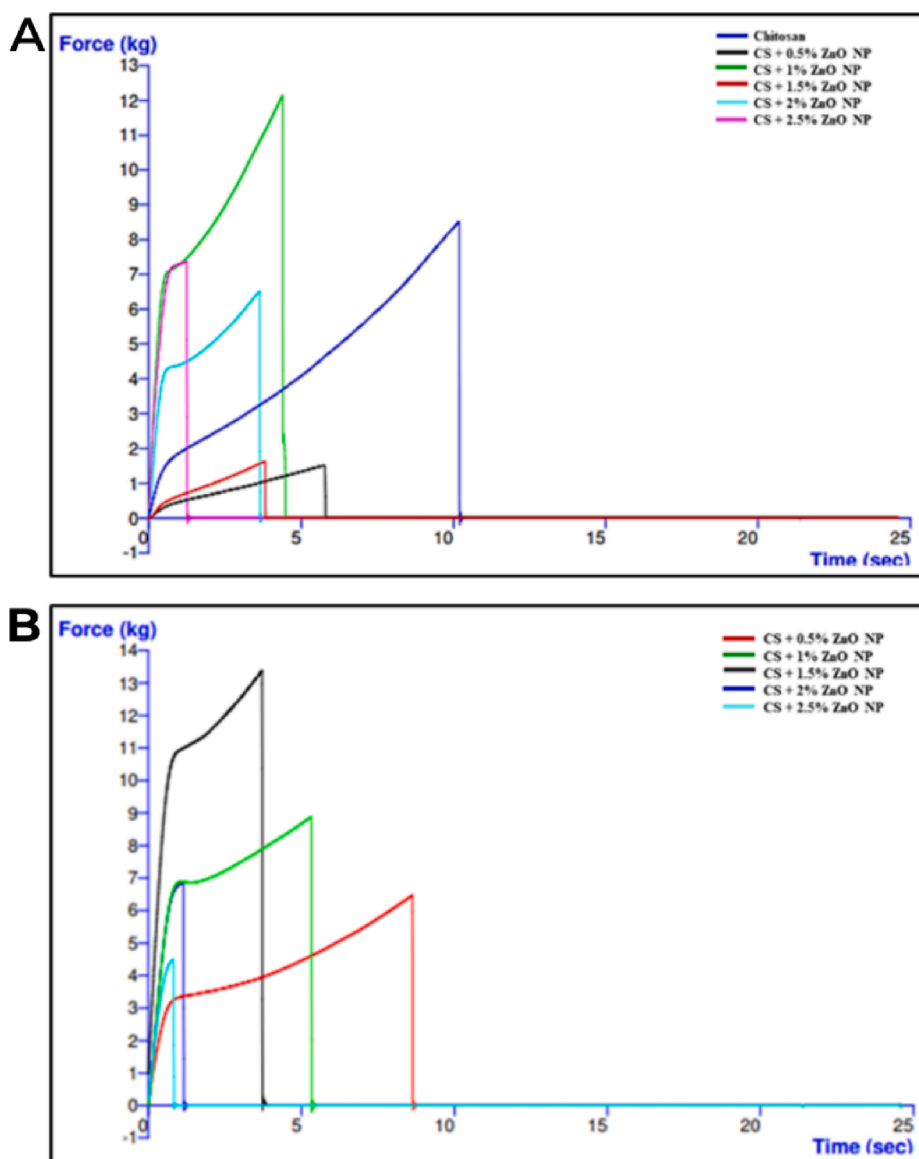


Fig. 8. Graph of force against time of (A) biogenic (B) chemogenic biofilms.

ZnO nanoparticles (at concentrations from 0.5% to 2.5%) to the chitosan matrix did not impact film uniformity. Higher ZnO NP concentrations in chitosan increased surface roughness due to uneven dispersion, with white spots indicating NP aggregation in micrographs. Intermolecular H-bonding between ZnO NPs and chitosan creates a dense structure (Gasti et al., 2022). Biogenic films have less aggregation than chemogenic films and using a compatible polymeric binder can prevent nanoparticle aggregation in nanocomposites (Kaushik et al., 2010).

3.3.2. Tensile grip

As shown in Fig. 8 are the graphs of force against time of pristine chitosan, biogenic, and chemogenic films. Chitosan is most elastic without ZnO NP, showing the longest time to break. Increasing ZnO NP concentrations contribute to rougher and thicker films, resulting in decreased elasticity. Results showed the elongation break of 0.5% and 1% of chemogenic films was longer as compared to biogenic films. However, 1%, 1.5%, 2%, and 2.5% of biogenic films had a longer elongation break point than chemogenic films. The incorporation of ZnO NPs in the chitosan matrix led to agglomeration, disrupting the crystalline structure and hindering bonding interactions. This resulted in decreased tensile grip in the films (Liu et al., 2021).

3.3.3. Film moisture

Good food preservation requires low FM (Bhat et al., 2023; Jha, 2020). Chitosan is naturally hydrophilic and prone to water absorption. The addition of nanoparticles effectively reduces FM (Souza et al., 2020b). Results showed the moisture content was highest in chitosan, followed by chemogenic 0.5%, 1%, 1.5%, 2%, and 2.5% biofilm, and lastly biogenic 0.5%, 1%, 1.5%, 2%, and 2.5% films. The synergistic relation between ZnO NPs and CS groups prevents water absorption, resulting in effective moisture reduction (Jha, 2020).

3.3.4. Film solubility

A nanocomposite with low FS provides a strong water barrier, preventing food spoilage and inhibiting microbe growth by blocking vapor entry into packaging (Aider, 2010). Based on Table 2, the FS was highest in chitosan, followed by chemogenic 0.5%, 1%, 1.5%, 2%, and 2.5% films, and lastly biogenic 0.5%, 1%, 1.5%, 2%, and 2.5% films. Increasing ZnO NP addition lowers FS by reducing available hydrophilic groups that interact with solvent molecules. ZnO NPs cross-link with chitosan chains via hydrophilic functional groups (Jayachandran et al., 2021b). This was also because the disruption of the chitosan-nanoparticle interface, coupled with intermolecular attraction,

Table 2

The average percentage of FS, FM, and WHC of biogenic, and chemogenic biofilms.

Films	Average Percentage (%)		
	Film Solubility	Film Moisture	Water-holding Capacity
Biogenic			
CS	28.361 ± 0.0352	18.771 ± 0.0426	31.698 ± 0.0191
CS + 0.5%ZnO NP	18.031 ± 0.0114	10.220 ± 0.0434	9.175 ± 0.0221
CS + 1%ZnO NP	14.823 ± 0.0164	12.732 ± 0.0397	7.842 ± 0.0269
CS + 1.5%ZnO NP	9.807 ± 0.0311	4.991 ± 0.0294	4.999 ± 0.0194
CS + 2%ZnO NP	5.804 ± 0.0126	5.318 ± 0.0302	5.315 ± 0.0273
CS + 2.5%ZnO NP	2.731 ± 0.0153	3.814 ± 0.0222	3.811 ± 0.0481
Chemogenic			
CS + 0.5% ZnO NP	16.811 ± 0.0342	14.362 ± 0.0356	14.141 ± 0.0161
CS + 1% ZnO NP	16.499 ± 0.0251	13.282 ± 0.0261	15.603 ± 0.0152
CS + 1.5% ZnO NP	12.743 ± 0.0383	9.103 ± 0.0234	9.961 ± 0.0173
CS + 2% ZnO NP	5.511 ± 0.0131	6.408 ± 0.0392	8.455 ± 0.0336
CS + 2.5% ZnO NP	3.914 ± 0.0332	4.364 ± 0.0181	5.352 ± 0.0411

restores the chitosan matrix by binding to hydroxyl groups (Zhang & Rhim, 2022).

3.3.5. Water-holding capacity

Natural polymers inherently retain water but adding nanoparticles in nanocomposites reduces WHC, preventing foodborne pathogen growth (Aider, 2010). This capacity is linked to porosity and total surface area, with higher porosity providing a larger surface area and increased WHC (Mahdi Ismail et al., 2023). Based on Table 2, the WHC was highest in chitosan, followed by chemogenic 0.5%, 1%, 1.5%, 2%, and 2.5% films, and lastly biogenic 0.5%, 1%, 1.5%, 2%, and 2.5% films. The addition of ZnO NPs to the chitosan matrix reduces WHC in the bio-nanocomposite, forming a three-dimensional ZnO network. ZnO NPs can absorb water due to the presence of hydroxide ions on their surface (Souza et al., 2019). The average percentage of FS, FM, and WHC of biogenic, and chemogenic biofilms is tabulated in Table 2.

4. Conclusion

This study demonstrated that ZnO NPs have been successfully synthesized using a feasible, rapid, cost-saving, eco-friendly bio-synthesis approach using waste banana (*Musa acuminata*) aqueous leaf extract. The aqueous leaf extract worked as the reducing, capping, and stabilizing agent throughout the green synthesis. The unique characteristics of ZnO NPs were confirmed using the standard characterization techniques: UV-Visible, XRD, SEM, EDX, and FTIR. The highest UV-Vis peak in both biogenic and chemogenic ZnO NP was found at 370 nm and 381 nm having sizes of 36.73 nm and 75.31 nm respectively. Both the biogenic and chemogenic ZnO NP were spherical at their highest purity. The biogenic ZnO NP exhibited a larger surface area which enhanced an inhibitory effect to kill foodborne bacteria (*S. typhimurium*, and *S. aureus*). Moreover, the biogenic films showed enhanced physico-chemical properties as compared to chemogenic films and pristine chitosan. The successful biogenic ZnO NP has superior properties to chemogenic ZnO NP. Hence, this study repurposed banana leaf agro-waste into novel materials for eco-friendly food packaging, promoting a circular green economy.

Declaration of Competing Interest

The authors declare that they have no known competing financial interests or personal relationships that could have appeared to influence

the work reported in this paper.

Acknowledgments

This study was supported by the Fundamental Research Grant Scheme, Ministry of Higher Education (MOHE) (FRGS/1/2021/STG02/UTAR/02/2).

References

- Abdul Razak, A.M., Raja Othman, R.N., Abdullah, M.F., Ku Ahmad, K.Z., 2021. An overview of banana biomass as a potential renewable energy source in Malaysia. *Jurnal Kejuruteraan si4* (1), 181–191. [https://doi.org/10.17576/jkukm-2021-si4\(1\)-23](https://doi.org/10.17576/jkukm-2021-si4(1)-23).
- Aider, M. (2010). Chitosan application for active bio-based films production and potential in the food industry: Review. In *LWT* (Vol. 43, Issue 6, pp. 837–842). Academic Press. <https://doi.org/10.1016/j.lwt.2010.01.021>.
- Alzate Acevedo, S., Díaz Carrillo, A. J., Flórez-López, E., & Grande-Tovar, C. D. (2021). Recovery of Banana Waste-Loss from Production and Processing: A Contribution to a Circular Economy. In *Molecules* (Basel, Switzerland) (Vol. 26, Issue 17). NLM (Medline). <https://doi.org/10.3390/molecules26175282>.
- Azim, Z., Singh, N. B., Khare, S., Singh, A., Amist, N., Niharika, & Yadav, R. K. (2022). Green synthesis of zinc oxide nanoparticles using Vernonia cinerea leaf extract and evaluation as nano-nutrient on the growth and development of tomato seedling. *Plant Nano Biology*, 2, 100011. <https://doi.org/10.1016/j.plana.2022.100011>.
- Basnet, P., Inakhumbi Chanu, T., Samanta, D., Chatterjee, S., 2018. A review on bio-synthesized zinc oxide nanoparticles using plant extracts as reductants and stabilizing agents. *J. Photochem. Photobiol. B Biol.* 183, 201–221. <https://doi.org/10.1016/j.jphotobiol.2018.04.036>.
- Bhat, V.G., Masti, S.P., Narasagoudar, S.S., Chougale, R.B., Kumar, P., Vantamuri, A.B., 2023. Development and characterization of Chitosan/Guar gum /Gum ghatti bionanocomposites with in situ silver nanoparticles. *Chem. Data Collect.* 44 <https://doi.org/10.1016/j.cdc.2023.101009>.
- Emamifar, A., Kadivar, M., Shahedi, M., Soleimani-Zad, S., 2010. Evaluation of nanocomposite packaging containing Ag and ZnO on shelf life of fresh orange juice. *Innov. Food Sci. Emerg. Technol.* 11 (4), 742–748. <https://doi.org/10.1016/j.ifset.2010.06.003>.
- Gasti, T., Dixit, S., Hiremani, V.D., Chougale, R.B., Masti, S.P., Vootla, S.K., Mudigoudra, B.S., 2022. Chitosan/pullulan based films incorporated with clove essential oil loaded chitosan-ZnO hybrid nanoparticles for active food packaging. *Carbohydr. Polym.* 277 <https://doi.org/10.1016/j.carbpol.2021.118866>.
- Imade, E.E., Ajiboye, T.O., Fadiji, A.E., Onwudiwe, D.C., Babalola, O.O., 2022. Green synthesis of zinc oxide nanoparticles using plantain peel extracts and the evaluation of their antibacterial activity. *Scientific African* 16. <https://doi.org/10.1016/j.sciaf.2022.e01152>.
- Jayachandran, A., T.R., A., & Nair, A. S. (2021b). Green synthesis and characterization of zinc oxide nanoparticles using Cayratia pedata leaf extract. *Biochemistry and Biophysics Reports*, 26. <https://doi.org/10.1016/j.bbrep.2021.100995>.
- Jha, P., 2020. Effect of plasticizer and antimicrobial agents on functional properties of bionanocomposite films based on corn starch-chitosan for food packaging applications. *Int. J. Biol. Macromol.* 160, 571–582. <https://doi.org/10.1016/j.ijbiomac.2020.05.242>.
- Kalpana, V. N., & Devi Rajeswari, V. (2018). A Review on Green Synthesis, Biomedical Applications, and Toxicity Studies of ZnO NPs. In *Bioinorganic Chemistry and Applications* (Vol. 2018). Hindawi Limited. <https://doi.org/10.1155/2018/3569758>.
- Kaushik, A., Singh, M., Verma, G., 2010. Green nanocomposites based on thermoplastic starch and steam exploded cellulose nanofibrils from wheat straw. *Carbohydr. Polym.* 82 (2), 337–345. <https://doi.org/10.1016/j.carbpol.2010.04.063>.
- Liu, J., Huang, J., Hu, Z., Li, G., Hu, L., Chen, X., Hu, Y., 2021. Chitosan-based films with antioxidant of bamboo leaves and ZnO nanoparticles for application in active food packaging. *Int. J. Biol. Macromol.* 189, 363–369. <https://doi.org/10.1016/j.ijbiomac.2021.08.136>.
- Mahdi Ismail, S.M., Ahmed, S.M., Abdulrahman, A.F., AlMessiere, M.A., 2023. Characterization of green synthesized ZnO nanoparticles by using pinus brutia leaves extracts. *J. Mol. Struct.* 1280 <https://doi.org/10.1016/j.molstruc.2023.135063>.
- Mohd Taib, R., Abdullah, N., & Azman Miskam, M. (2014). Characterization of Banana (*Musa spp.*) Pseudo-Stem and Fruit-Bunch-Stem as a Potential Renewable Energy Resource Characteristics of graphene produce from biochar View project Bioenergy and Biofuels study View project. <https://www.researchgate.net/publication/265051818>.
- Rahman, P.M., Mujeeb, V.M.A., Muraleedharan, K., 2017. Flexible chitosan-nano ZnO antimicrobial pouches as a new material for extending the shelf life of raw meat. *Int. J. Biol. Macromol.* 97, 382–391. <https://doi.org/10.1016/j.ijbiomac.2017.01.052>.
- Souza, V.G.L., Pires, J.R.A., Vieira, É.T., Coelho, I.M., Duarte, M.P., Fernando, A.L., 2019. Activity of chitosan-montmorillonite bionanocomposites incorporated with rosemary essential oil: From in vitro assays to application in fresh poultry meat. *Food Hydrocoll.* 89, 241–252. <https://doi.org/10.1016/j.foodhyd.2018.10.049>.
- Tan, B.C., 2022. Can Banana be a Success Story for Malaysia? *J. Agribusiness Marketing* 9 (1), 13–22. <https://doi.org/10.56527/jabm.9.1.2>.
- Tan, Y.Y., Wong, L.S., Nyam, K.L., Wittayanarakul, K., Zawawi, N.A., Rajendran, K., Djearmane, S., Dhanapal, A.C.T.A., 2023. Development and Evaluation of Topical

- Zinc Oxide Nanogels Formulation Using *Dendrobium anosmum* and Its Effect on Acne Vulgaris. *Molecules* 28, 6749. <https://doi.org/10.3390/molecules28196749>.
- Terzioğlu, P., Güney, F., Parın, F.N., Şen, I., Tuna, S., 2021. Biowaste orange peel incorporated chitosan/polyvinyl alcohol composite films for food packaging applications. *Food Packag. Shelf Life* 30. <https://doi.org/10.1016/j.fpsl.2021.100742>.
- Velumani, M., Thirupathi, G., Mohankumar, A., Kalaiselvi, D., Sundararaj, P., Premasudha, P., 2022. Green synthesis of zinc oxide nanoparticles using *Cananga odorata* essential oil and its antibacterial efficacy in vitro and in vivo. *Comparative Biochem. Physiol. Part - C: Toxicol. Pharmacol.* 262 <https://doi.org/10.1016/j.cbpc.2022.109448>.
- Zhang, W., & Rhim, J. W. (2022). Functional edible films/coatings integrated with lactoperoxidase and lysozyme and their application in food preservation. In *Food Control* (Vol. 133). Elsevier Ltd. <https://doi.org/10.1016/j.foodcont>.